

Multiple equilibria in a cloud-resolving model using the weak temperature gradient approximation

Sharon L. Sessions,¹ Satomi Sugaya,¹ David J. Raymond,¹ and Adam H. Sobel²

Received 13 October 2009; revised 29 January 2010; accepted 19 February 2010; published 19 June 2010.

[1] Multiple equilibria corresponding to either a state with persistent, precipitating deep convection or a nonprecipitating state are shown to exist in a cloud-resolving model employing the weak temperature gradient (WTG) approximation. WTG is important for the existence of both equilibria; numerical experiments show that a weak enforcement of WTG eliminates the dry nonprecipitating state. In situations which support both equilibria, we find that the dry equilibrium has a small or negative gross moist stability, while larger positive values of gross moist stability correspond to the precipitating equilibrium. Our simulations also show that the gross moist stability tends to become negative during times of rapid change in the atmospheric moisture, as occurs in the transient stages of convection.

Citation: Sessions, S. L., S. Sugaya, D. J. Raymond, and A. H. Sobel (2010), Multiple equilibria in a cloud-resolving model using the weak temperature gradient approximation, *J. Geophys. Res.*, 115, D12110, doi:10.1029/2009JD013376.

1. Introduction

[2] Recent work by Sobel *et al.* [2007] (hereafter SBB07) has demonstrated the existence of multiple equilibria in a single column model of the atmosphere using the weak temperature gradient (WTG) approximation with parameterized deep convection. They showed that in conditions with sufficient convective available potential energy (CAPE) for convection to occur, an initially dry column would remain dry unless some mechanism (such as horizontal moisture advection) sufficiently moistened the free troposphere. This work is directly related to multiple equilibria of the Hadley circulation [Bellon and Sobel, 2010], which suggests that understanding this phenomenon in limited-domain simulations may be important to understanding the interaction between convection and large-scale dynamics in the tropics.

[3] In this work, we pursue the idea that multiple equilibrium states may exist in the atmosphere by performing numerical experiments with a cloud-resolving model (CRM) which interacts with the implicit large-scale circulations in a parameterized way via the WTG approximation. We demonstrate that multiple equilibrium states do exist in our model, but only under strict conditions which depend on surface fluxes (controlled by either imposed surface winds or sea surface temperatures (SSTs)), domain size, and the time scale with which the local vertical profiles of potential temperature relax to that of the large-scale environment. The equilibrium state which is realized by the model depends on the initial moisture in the modeled domain, which is consistent with the results from SBB07.

[4] In addition to determining the conditions for the existence of multiple equilibria within our model, we investigate the gross moist stabilities of the transient and steady states. We find that the gross moist stability is a particularly important parameter not only for diagnosing the environment in either equilibrium, but in characterizing the development of deep convection.

[5] Since the WTG approximation and gross moist stability are both important concepts in this paper, we review these in sections 1.1 and 1.2. Our numerical experiments are described in section 2; results are presented in section 3. The role of gross moist stability in the context of multiple equilibria is discussed in section 4. Finally, section 5 includes a general discussion and summary.

1.1. WTG in the Model

[6] We run a version of the cloud-resolving model very similar to that described by Raymond and Zeng [2005] (hereafter RZ05). The model implements the WTG approximation as described by RZ05, which is based on the original ideas of Sobel and Bretherton [2000] (hereafter SB00). The basic premise of WTG is that the potential temperature in the tropics tends to be horizontally homogeneous, and any buoyancy anomalies produced by surface heat fluxes, latent heat release or radiation redistribute quickly by means of gravity waves [Bretherton and Smolarkiewicz, 1989; Mapes and Houze, 1995]. This redistribution maintains the horizontal homogeneity in the temperature profiles. In the model, this effect is achieved by the imposition of a hypothetical vertical velocity, called the WTG velocity (w_{wtg}), which produces vertical advection of potential temperature sufficient to counteract the effects of heating.

[7] As we will demonstrate in section 3, the WTG approximation plays an important role in the existence of multiple equilibria in our model. Consequently, we will briefly highlight some of the details of implementation in our model. For a more thorough discussion, see RZ05. In the

¹Department of Physics and Geophysical Research Center, New Mexico Institute of Mining and Technology, Socorro, New Mexico, USA.

²Department of Applied Physics and Applied Mathematics and Department of Earth and Environmental Sciences, Columbia University, New York, New York, USA.

model, the total wind field, \mathbf{v}_T , is composed of a part that is computed explicitly by the model and a part that is generated to maintain the WTG approximation (\mathbf{v} and \mathbf{v}_{wtg} , respectively),

$$\mathbf{v}_T = \mathbf{v} + \mathbf{v}_{\text{wtg}}. \quad (1)$$

Each of the contributions satisfy mass continuity individually. The first contribution obeys cyclic boundary conditions on the lateral model boundaries, which implies that its contribution to the domain averaged vertical mass flux is zero. The second contribution has horizontal and vertical components, $\mathbf{v}_{\text{wtg}}^h$ and w_{wtg} , which satisfy the anelastic mass continuity equation,

$$\nabla \cdot (\bar{\rho} \mathbf{v}_{\text{wtg}}^h) + \frac{\partial(\bar{\rho} w_{\text{wtg}})}{\partial z} = 0, \quad (2)$$

where $\bar{\rho}(z)$ is the horizontally averaged density. w_{wtg} is taken to be horizontally uniform, and a horizontal average of $\mathbf{v}_{\text{wtg}}^h$ is assumed to be zero at each level. We postulate that $|\mathbf{v}| \gg |\mathbf{v}_{\text{wtg}}^h|$, and thus the approximate treatment of \mathbf{v}_{wtg} above is justified.

[8] The equation for potential temperature, θ , implemented in the model is

$$\frac{\partial(\rho\theta)}{\partial t} + \nabla \cdot (\rho \mathbf{v} \theta + \mathbf{T}_\theta) \equiv \rho(S_\theta - E_\theta). \quad (3)$$

Here, \mathbf{T}_θ represents unresolved eddy and viscous transport, S_θ is the diabatic potential temperature source, and E_θ enforces the WTG approximation via a relaxation of the potential temperature to a reference profile $\theta_0(z)$,

$$E_\theta = w_{\text{wtg}} \frac{\partial \bar{\theta}}{\partial z} = \sin(\pi z/h) \frac{\{\bar{\theta} - \theta_0(z)\}}{t_\theta}. \quad (4)$$

The overbar indicates a horizontal average of potential temperature, h is the height of the tropopause, and t_θ is the time over which the vertical profile of potential temperature relaxes to the specified reference profile. Note the sinusoidal modulation of the potential temperature in the vertical. This is to emphasize the role of gravity waves in adjusting the buoyancy in the middle troposphere. Above the tropopause, the relaxation rate (t_θ^{-1}) is set to zero. Also, since WTG breaks down in the boundary layer [Sobel and Bretherton, 2000], the value at the top of the boundary layer (taken to be 1000 m) is linearly interpolated to zero at the surface.

[9] The equation for total water mixing ratio, r_t , is given by

$$\frac{\partial(\rho r_t)}{\partial t} + \nabla \cdot (\rho \mathbf{v} r_t + \mathbf{T}_r) \equiv \rho(S_r - E_r), \quad (5)$$

where \mathbf{T}_r represents unresolved eddy and viscous transport, S_r is the source of r_t due to precipitation and evaporation, and E_r is an approximation which represents the entrainment of total advected water from the environment and the vertical transport of water by the large-scale vertical motion. Specifically,

$$E_r = \frac{(\bar{r}_t - r_x)}{\bar{\rho}} \frac{\partial(\bar{\rho} w_{\text{wtg}})}{\partial z} + w_{\text{wtg}} \frac{\partial \bar{r}_t}{\partial z}. \quad (6)$$

Here, r_x equals the reference profile $r_0(z)$ when $\partial(\bar{\rho} w_{\text{wtg}})/\partial z > 0$ and is equal to \bar{r}_t otherwise. This assignment assures that the outflowing air has a total water mixing ratio equal to the horizontal average in the domain (i.e., \bar{r}_t), while inflowing air has a mixing ratio representative of the environment surrounding the domain which is specified by the reference profile, $r_0(z)$. We note that equation (2) has been used to derive equation (6). For more details, see RZ05.

[10] As described by RZ05, the WTG velocity substantially modifies the evolution of convection. As equation (4) shows, the model does not strictly impose a background profile of potential temperature, but rather allows the instantaneous local profile to relax to a reference profile equal to the assumed large-scale mean over a time scale t_θ . Physically, we interpret t_θ to be the amount of time it takes a gravity wave to cross the modeled domain. Though we may set this time scale according to realistic gravity wave speeds for a given domain size (e.g., a gravity wave traveling at 50 m s^{-1} would take approximately 33 min to cross a 100 km domain), we vary this parameter to investigate the response of the modeled convection. Furthermore, we may think of this relaxation time scale as a measure of the strength with which the weak temperature gradient approximation is enforced: $t_\theta = 0$ corresponds to strict enforcement of WTG ($\bar{\theta} \equiv \theta_0(z)$ in equation (4); this was used by SB00 and SBB07) while $t_\theta = \infty$ turns off WTG mode in the simulations and allows the model to evolve toward radiative convective equilibrium. The tropical environment falls somewhere in between these two extremes, depending on the time and space scales of interest.

[11] The model used in these simulations prescribes only the potential temperature relaxation time. This parameter controls the corresponding WTG vertical velocity which vertically advects moisture. Horizontal advection of moisture from the surrounding environment is determined by assuming that the advecting velocity is purely divergent, so that it can be computed self-consistently from the WTG vertical velocity using mass continuity (RZ05 and equation (2)). This is equivalent to simulating a Lagrangian column moving at the prescribed wind speeds. SBB07, on the other hand, specified the time scale for horizontal advection of moisture a priori. This can be thought of as an assumption that the rotational component of the advecting horizontal velocity is much larger than the divergent component, so that the latter can be neglected and the horizontal advection of moisture is decoupled from the WTG vertical velocity. SBB07 showed that the existence of multiple equilibria is sensitive to the moisture relaxation, and thus an important question arises: Does the existence of multiple equilibria depend on relaxation of the vertical profile of potential temperature or moisture? Because the horizontal advection time scale is not specified externally here, but rather determined interactively from the WTG vertical velocity, we cannot disentangle these effects and thus we do not address this question in the present study.

1.2. Normalized Gross Moist Stability

[12] The gross moist stability can be thought of as a measure of precipitation efficiency. It was first introduced by Neelin and Held [1987] as a means to model tropical convergence based on the moist static energy budget (moist static energy being approximately conserved in moist processes). In

this work, we choose to use the convention of *Raymond et al.* [2007], which defines the normalized gross moist stability (NGMS) in terms of moist entropy (which is also approximately conserved in moist processes). Specifically, we define Γ to be the NGMS,

$$\Gamma = \frac{T_R[\nabla \cdot (s\mathbf{v})]}{-L[\nabla \cdot (r\mathbf{v})]} = \frac{T_R \frac{1}{g} \int \nabla \cdot (s\mathbf{v}) dp}{-L \frac{1}{g} \int \nabla \cdot (r\mathbf{v}) dp}, \quad (7)$$

where s is the moist entropy, r is the total water mixing ratio, and \mathbf{v} is the horizontal wind. The square brackets indicate a vertical pressure integral over the troposphere, g is the gravitational acceleration, and ∇ is the horizontal divergence operator. T_R and L are a constant reference temperature and the latent heat of condensation, which are included so that Γ is dimensionless. We thus define NGMS as the ratio of the vertically integrated lateral moist entropy export to moisture import. In a majority of cases, NGMS is a positive quantity, but can become negative if moist entropy and moisture are both imported into (or exported from) a convecting region.

[13] Observations suggest that the sign of NGMS in a convecting region is related to the level of nondivergence in the horizontally averaged circulation [*López-Carrillo and Raymond, 2005; Back and Bretherton, 2006*]. In particular, when convergence is concentrated at low levels, as expected in the early stages of the development of deep convection, a vertical pressure integral of moist entropy or moist static energy divergence gives a net import of these quantities. Coupled with the moisture convergence, this results in a negative NGMS. In a region of subsidence, we expect moisture export, and either a modest import or export of moist entropy. The latter also results in a negative NGMS. As we will show in section 4, both of these situations are realized in our model.

[14] A thorough discussion on the role of NGMS in tropical dynamics is given by *Raymond et al.* [2009]. As in the work of *Raymond et al.* [2007], the net precipitation in the steady state is related to the NGMS according to

$$L\Gamma(P - E) = T_R(F_s - R), \quad (8)$$

where P is the precipitation rate, E is the surface evaporation rate, F_s is the surface moist entropy flux due to surface heat and moisture fluxes, and R is the pressure integral of the entropy sink per unit mass due to radiation divided by the acceleration of gravity. Equation (8) suggests that the net precipitation ($P - E$) is inversely proportional to the NGMS for a given net entropy forcing. This is consistent with the results from *Raymond and Sessions* [2007], which showed that thermodynamic profiles which are either moister or more unstable at low levels result in smaller values of NGMS and increased precipitation rates. The results described in section 4 are consistent with those findings, and demonstrate that NGMS can be used as a diagnostic for characterizing the equilibrium state of the system.

2. Experiments

[15] For the implementation of the WTG approximation, we must specify the vertical profiles of potential temperature and mixing ratio representing the large-scale environmental mean. For simplicity, we take this reference profile to be

one of radiative convective equilibrium (RCE), generated by averaging the last 3×10^6 s (~ 35 days) in a 5×10^6 s (~ 58 days) non-WTG simulation (i.e., $t_\theta = \infty$). RCE profiles are generated with imposed horizontal surface wind speeds of 5 m s^{-1} over tropical oceans with SSTs of 303 K. The horizontal wind is perpendicular to the two-dimensional plane of the domain (all simulations are in two dimensions to decrease the computational demand). The simple radiative model used by *Raymond and Zeng* [2000] calculates radiative cooling interactively in these simulations.

[16] We have found that the RCE profiles are sensitive to the domain size and we thus perform RCE simulations for each domain size and grid resolution used in the numerical experiments. The vertical domain size used in the experiments is 20 km with a 250 m vertical resolution. We used horizontal domain sizes of 50, 100 or 200 km. The 100 and 200 km domains had a horizontal resolution of 1 km (to reduce computational expense). Most of the 50 km domains used a horizontal grid resolution of 500 m, though several experiments used a 1 km grid to facilitate comparisons with the larger domains. Unless otherwise noted, all references to the 50 km domain correspond to runs with a 500 m resolution.

[17] Figures 1a and 1b show a comparison between the horizontal and temporal averages of potential temperature and mixing ratio of the RCE simulations. To emphasize the differences, we plot the deviations of all profiles from the 50 km domain size with 500 m resolution. The differences between the logarithm of the mixing ratios is shown in Figure 1c to exaggerate the differences in the moisture content of the upper troposphere. The solid curves correspond to 50 km domains with line thickness indicating grid resolution (thin and thick curves correspond to 500 m and 1 km resolution, respectively). Dashed and dotted curves show deviations of the 100 km and 200 km domains from the 50 km domain. Note that the larger domains are slightly warmer and drier in the free troposphere (from about 2.5 to 12 km; Figures 1a and 1b) than the 50 km domains, though the 50 km domain with coarser resolution is considerably drier just above the boundary layer (1–2.5 km).

[18] We do not fully understand the origin of these differences, though a comparison of the fractional coverage of precipitating clouds for the different RCE simulations may provide one possible explanation. Comparing the effects of grid resolution on the 50 km domains, we find that the finer grid produces a considerably moister domain with precipitating clouds covering a larger fraction of the space-time domain ($18.5 \pm 1.1\%$ versus $14.7 \pm 0.9\%$ of the domain has a precipitation rate of at least 1 mm d^{-1}). The larger domains have a slightly lower fractional coverage ($13.1 \pm 0.7\%$ and $13.1 \pm 0.6\%$ with precipitation rate of at least 1 mm d^{-1} for the 100 and 200 km domains, respectively), which suggests that there is more room for descent to exist. This in turn allows the domain to warm and dry slightly compared to the smaller domains. In section 3, we show that the differences in the RCE reference profiles have essentially no effect on the WTG runs with 1 km grid resolution, but that the moister profile associated with the finer resolution produces slightly higher precipitation rates (e.g., see Figures 3 and 4 in section 3.1).

[19] Having specified the reference profile for the WTG simulations, we now describe the parameters in the modeled domain. We choose to fix the sea surface temperature at 303 K, and vary the strength of the surface horizontal wind.

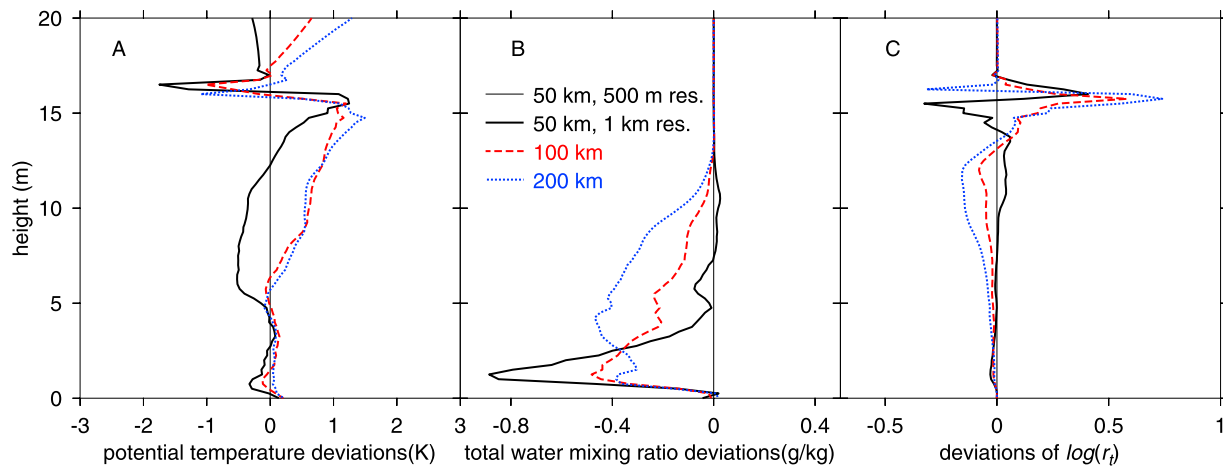


Figure 1. Comparison of RCE profiles for 50, 100, and 200 km domains (solid, dashed, and dotted curves, respectively). To emphasize the difference between the profiles characterizing the large-scale environment, we plot the deviations of the profiles from those of the 50 km domain with 500 m resolution (thin solid curve). (a) Deviations in potential temperature, (b) deviations in total water mixing ratio, and (c) the differences in the log of the mixing ratio are shown to emphasize the differences in moisture in the upper troposphere. The larger domains are warmer in the upper troposphere but are also considerably drier. Note the difference in moisture distribution for the 50 km domains (line thickness denotes grid resolution).

For each experiment, the wind speed is specified and approximately maintained throughout the duration of the simulation. Both SST and surface winds control surface fluxes, with larger values producing more convection and correspondingly greater precipitation rates (e.g., RZ05 and SBB07). In these experiments, the prescribed surface wind ranges from 0 to 20 m s⁻¹, with most runs set at 5, 7, 10 or 15 m s⁻¹.

[20] As discussed in section 1.1, we also vary the time scale of relaxation of potential temperature toward the large-scale mean. This effectively controls the degree to which the model obeys the WTG approximation, and consequently controls the magnitude of the WTG vertical velocity. By mass continuity, this fixes the horizontal flow and controls the horizontal advection of moisture from the surrounding environment.

[21] Each experiment is initiated with vertical profiles of potential temperature and total water mixing ratio which may differ from the RCE reference profile. The initial mixing ratio profile is taken to be

$$r_{i(\text{init})}(z) = f r_{i0}(z), \quad (9)$$

where $r_{i0}(z)$ is the RCE profile which represents the surrounding environment, and f is a fractional multiplier ($0 \leq f \leq 1$). Initializing the domain with the moisture content of the surrounding environment corresponds to $f = 1$, while a domain that is initially completely dry has $f = 0$. Only $f = 0, 1$ were used by SBB07. In addition to these extremes, we perform some experiments with the initial moisture of the modeled domain as some fraction of the RCE profile ($0 < f < 1$).

[22] The initial potential temperature profile is given by

$$\theta_{\text{init}} = \theta_0(1 + \delta\theta_{\text{local}}/\theta_0)(1 + \delta\theta_{\text{random}}/\theta_0), \quad (10)$$

where θ_0 is the RCE profile used to represent the large-scale mean, $\delta\theta_{\text{local}}$ and $\delta\theta_{\text{random}}$ represent localized and random perturbations, respectively (see Appendix A for details on the

perturbations). A limited number of simulations which vary $\delta\theta_{\text{local}}$ and $\delta\theta_{\text{random}}$ were performed to determine the sensitivity to initial conditions. Preliminary results suggest that the final state of the system is not very sensitive to these perturbations, though more investigation is necessary in order to determine this conclusively. We do note, however, that setting $\delta\theta_{\text{random}} = \delta\theta_{\text{local}} = 0$ and $f = 0$ will not generate convection no matter what the boundary conditions are.

[23] One of the primary goals of this paper is to characterize the statistically steady states of the system, which we assume with some confidence will remain stable indefinitely. The steady state precipitation and NGMS are taken as averages over the last month of the simulation. In most cases, the simulation was run for 4 months, though the run time varied from 60 to 364 days. (A data set of model parameters, including run times of each simulation is provided in the auxiliary material, Data Set S1.¹) The shorter runs were justified from the observation that once the model began precipitating, it equilibrated rather quickly (over a period of hours), and remained in a statistically steady state. For the numerical experiments which were initially dry, it could take several days or months to develop precipitation (in one case, this transition occurred after 70 days; see Figure 2). In those cases, longer run times may be necessary to observe a transition. For that reason, several experiments were run for a full year to verify whether the system would transition at a later time or if it was truly in a stable equilibrium. Of these, most remained completely dry for the duration of the model run. Two experiments showed moistening of the troposphere after 4 months which was insufficient to overcome convective inhibition and trigger deep convection, even after running the simulation for a full year.

[24] Finally, we note that despite some model runs of up to one year, we cannot exclude the possibility that convection

¹Auxiliary materials are available at <ftp://ftp.agu.org/apend/jd/2009jd013376>.

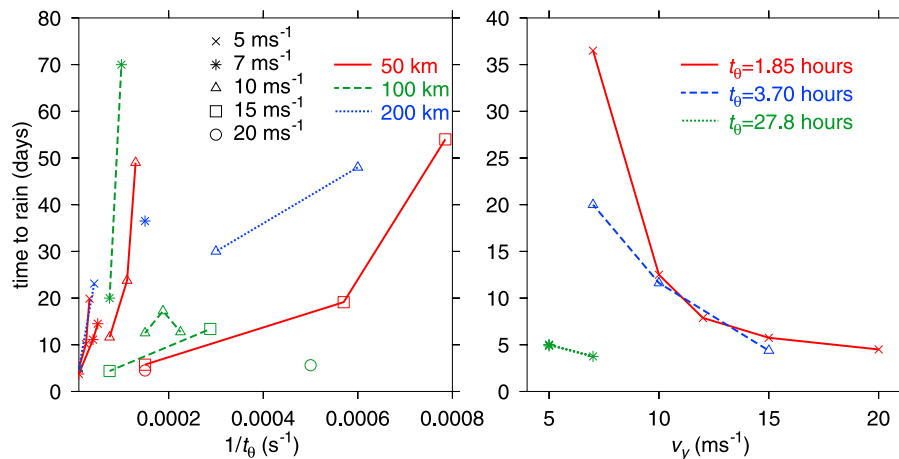


Figure 2. The amount of time needed for an initially dry domain to generate at least 1 mm d^{-1} precipitation rate is plotted as a function of (left) relaxation rate (t_θ^{-1}) and (right) surface wind speed (v_y). In the first case, curves connect experiments with same domain size (indicated by line style) and wind speed (symbols). Experiments shown on Figure 2 (right) had a common t_θ and thus allowed us to see how the imposed wind speed influenced the onset of precipitation (independent of domain size). Note the different scale on the vertical axes.

could still develop after the model run time. Indeed, of the initially dry experiments which eventually precipitated, we found that the amount of time it took to initiate precipitation increased with decreasing surface wind speeds and potential temperature relaxation time. This is shown in Figure 2. In Figure 2 (left) the amount of time it took for a precipitation rate of at least 1 mm d^{-1} to develop is plotted as a function of the relaxation rate (t_θ^{-1}) for different surface wind speeds and domain sizes. In all but one instance, the time to precipitate increased with decreasing t_θ , suggesting that a further decrease in t_θ (which corresponds to a stricter enforcement of WTG) would require a longer wait time to transition to the precipitating equilibrium for a given domain size and wind speed. Considering that the real atmosphere will not maintain steady conditions over a time scale of months, we do not give further consideration to this possibility. Also note that surface fluxes play a role in the amount of time required for precipitation to occur. As shown in Figure 2 (right), more vigorous surface fluxes associated with higher surface wind speeds initiate convection more quickly. In this case, if we consider wind speeds close to or below the values used to compute the RCE reference profile, we do not expect convection to initiate no matter how long we wait, since there will not be sufficient CAPE. The choice of a 4 month simulation is somewhat arbitrary, and is chosen in hopes that this gives initially dry atmospheres enough time to develop convection if they are going to do so, without excessive computation time.

3. Results

[25] As in work of SBB07, we perform parallel experiments with the domain initialized either with the moisture profile of the surrounding environment or completely dry. We then vary the boundary conditions (surface wind speed, domain size and WTG relaxation time) in each case to establish the range of conditions which support multiple equilibria. Upon establishing this range, we vary the initial

conditions to determine the sensitivity of the realized equilibrium to the initial state of the domain. The results from SBB07 suggest that the final equilibrium state depends on the initial moisture in the modeled domain. We cannot say a priori whether or not the system always evolves to the precipitating equilibrium state if some amount of moisture exists in the free troposphere, or if there is a minimum amount required to overcome convective inhibition. We address this issue in this section, as well as how this depends on the boundary conditions.

[26] In addition to determining the range of boundary conditions which support multiple equilibria, and the sensitivity of the final state to initial conditions, we consider the NGMS as a diagnostic for characterizing the equilibrium state of a modeled domain. Furthermore, we discuss the role of NGMS in developing (or decaying) convection as well as in the steady state. These results are shown in section 4.

3.1. Dependence on Surface Wind Speed

[27] The first set of experiments aims to determine the range of wind speeds which support multiple equilibria for a given domain size and potential temperature relaxation time (with SST fixed). Figure 3 shows results for a 50 km domain with $t_\theta = 1.85 \text{ h}$. Experiments initiated with RCE moisture profiles are indicated by circles (solid curve), while squares (dashed curve) represent initially dry experiments. Thin curves correspond to a grid resolution of 500 m, while thick curves give the 1 km grid results. Figure 3 is analogous to Figure 2 of SBB07, except that SBB07 fixed the wind speed and SSTs were varied compared to the RCE value. As discussed in section 2, both have the effect of modulating surface fluxes.

[28] From Figure 3 (top), we note that a single, precipitating equilibrium exists for wind speeds of 12 m s^{-1} and greater, regardless of horizontal grid resolution. For the finer (500 m) grid, a single nonprecipitating equilibrium exists below a wind speed of 5 m s^{-1} , while horizontal wind speeds from 5 to 10 m s^{-1} can sustain either a dry or a precipitating steady state,

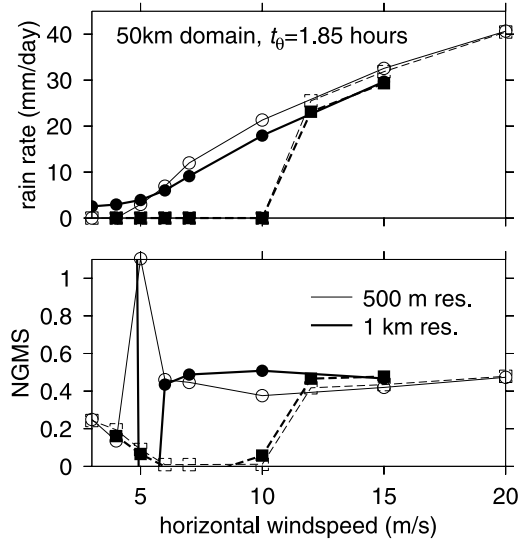


Figure 3. (top) Precipitation and (bottom) NGMS as a function of imposed horizontal wind speed. Solid curves (circles) represent simulations initiated with RCE profiles of potential temperature and mixing ratio. Simulations which were initially dry are shown with dashed curves (squares). Line thickness indicates horizontal grid resolution. In the range of 5 and 10 m s^{-1} , two equilibrium states exist regardless of grid resolution; above 10 m s^{-1} , only the precipitating state exists; below 5 m s^{-1} , only the dry state remains for the finer grid, while multiple equilibria persist at lower wind speeds for the coarser grid.

depending on the initial moisture profile. Specifically, in the range of wind speeds that can sustain multiple equilibria, an initially dry domain will remain dry, while an initially moist domain will sustain persistent convection. The only difference in the simulations is the initial mixing ratio profile, which is consistent with results of SBB07. Similar results also

hold for the coarser (1 km) grid, though multiple equilibria persist even for wind speeds as low as 3 m s^{-1} .

[29] These results demonstrate that multiple equilibrium states exist under certain boundary conditions in our CRM in the WTG approximation. As the wind speed is increased, surface fluxes overcome convective inhibition, allowing shallow convection to penetrate into the free troposphere thus effectively destroying the dry equilibrium state.

[30] Figure 3 (bottom) shows the steady state value of NGMS for the corresponding runs. The significance of these values will be discussed further in section 4.2.

[31] Experiments similar to those presented in Figure 3 on 100 and 200 km domains show similar behavior, with one important distinction: The larger the domain, the smaller the range in which multiple equilibria exist. Figure 4 shows that with a thermodynamic relaxation time of 1.85 h, there is only a very narrow range of wind speeds which permit multiple equilibrium on a 100 km domain, and this range decreases even more for a computational domain of 200 km. Also note that, unlike the coarsely gridded 50 km domain, the precipitating equilibrium is destroyed for wind speeds less than 5 m s^{-1} . We discuss the dependence on domain size below.

3.2. Dependence on Domain Size and Relaxation Time

[32] We did not systematically probe the dependence of precipitation rate on domain size for different relaxation rates, but in comparable instances, we found very little difference in the domain averaged precipitation rate as a function of wind speed in any of the domains with 1 km horizontal grid resolution and wind speeds of 5 m s^{-1} and greater (as discussed above, wind speed less than this sustained precipitation in the 50 km domain while other domain sizes dried and remained dry). Furthermore, there is only a slight difference between the results from a 1 km grid and the 500 m grid, with the finer grid producing slightly higher precipitation rates (compare Figures 3 and 4). As explained in section 2, we suspect that this difference is attributed to the moister RCE reference

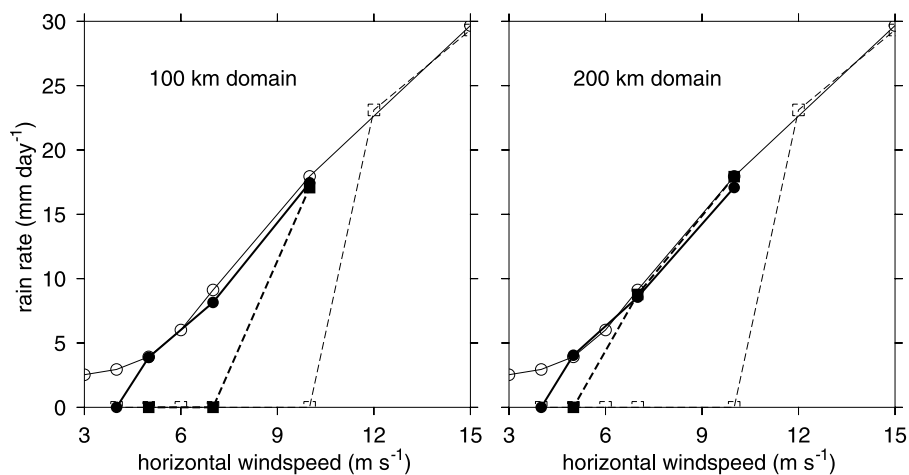


Figure 4. Same as Figure 3 (top) but for the (left) 100 and (right) 200 km domain experiments. The results for the 50 km domain with 1 km horizontal grid resolution have been overlaid with thin curves and open symbols for comparison. Note that the range of wind speeds where multiple equilibria exist decreases as the domain size increases.

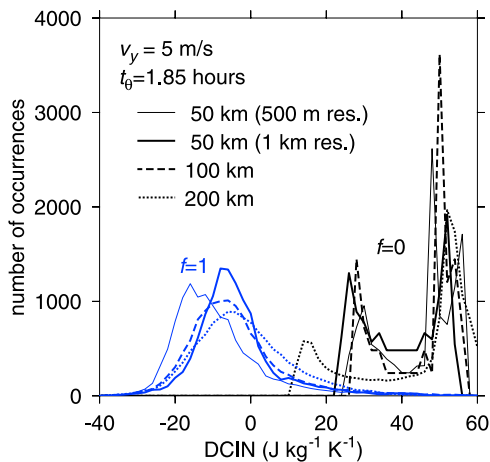


Figure 5. A histogram of values of DCIN (see text) for experiments with surface winds of 5 m s^{-1} and $t_\theta = 1.85 \text{ h}$. Line styles differentiate domain sizes and resolution. For these boundary conditions, all simulations which were initially dry remained dry ($f = 0$, on the right side), and runs initially moist sustained convection ($f = 1$, on the left side). Note that the $f = 0$ curve for the 200 km domain has a considerable number of low-DCIN points compared to the other domains.

profile generated with a finer grid resolution. Accounting for this, we conclude that in the convecting equilibrium state, there is little dependence of precipitation rate on domain size for a given wind speed and potential temperature relaxation time.

[33] Though the change in precipitation rate as a function of domain size in the precipitating equilibrium is nearly negligible, the role of domain size in determining the existence of multiple equilibria (as seen in Figure 4) is quite significant. Smaller computational domains allow multiple equilibria over a larger range of wind speeds. This dependence on domain size is at least partially related to the distribution of convective inhibition in the modeled domain. Figure 5 shows a histogram of deep convective inhibition (DCIN) [Raymond *et al.*, 2003], where DCIN is defined as

$$\text{DCIN} = s_t - s_b. \quad (11)$$

Here, s_t is the threshold entropy for convection and is defined as the vertical average of the saturated moist entropy over the height range 1750–2000 m; s_b is the boundary layer entropy defined as the average of moist entropy over 0–1000 m. The curves on the right in Figure 5 correspond to simulations which were initiated with dry mixing ratio profiles ($f = 0$ from equation (9)), while curves on the left correspond to simulations initiated with the RCE mixing ratio profiles ($f = 1$). For this set of boundary conditions, all simulations which were initially dry remained dry, and the values of DCIN were taken from the last month and over the entire domain of each simulation (the number of occurrences was normalized to account for a larger number of grid points on larger domain sizes). Even in runs which remained dry, the 200 km domain experienced a higher frequency of lower values of DCIN, which increases the possibility that convection will spontaneously initiate. Indeed, this does occur when the surface wind speed is increased from 5 to 7 m s^{-1} (see, e.g., Figure 4).

Though we believe that this contributes to the dependence of multiple equilibria on domain size, the similarity between the DCIN distributions in the 50 km and 100 km domains suggests that this is not the whole story.

[34] The results from SBB07 showed that the existence of multiple equilibrium states depends on the time scale of horizontal moisture advection. As we explained earlier, our model ties moisture advection to the time scale of the potential temperature relaxation in the WTG implementation via mass continuity. To explore the implications of this relation, we performed several experiments to determine the sensitivity of multiple equilibria with respect to the WTG potential temperature relaxation time, t_θ . Decreasing the value of t_θ is tantamount to decreasing the amount of time it takes to remove buoyancy anomalies in the vertical profile of potential temperature. A relaxation time of zero corresponds to an instantaneous relaxation to the specified environmental profile, and thus strictly enforces the WTG approximation, and $t_\theta = \infty$ turns off WTG entirely.

[35] Figure 6 illustrates the dependence of the final precipitation state on the potential temperature relaxation time for the different domain sizes. All of the experiments shown were initiated with zero moisture and have an imposed horizontal wind speed of 10 m s^{-1} . The larger values of t_θ result in a precipitating state, and all domain sizes can maintain a dry equilibrium for sufficiently small t_θ . This means that the more strongly the WTG approximation is enforced, the more likely the system is to sustain multiple equilibria. Furthermore, the relaxation time scale at which the dry equilibrium is destroyed decreases with increasing domain size. This implies that the WTG approximation must be more vigorously enforced the larger the domain in order to maintain multiple equilibria. To rationalize this tendency, consider that smaller relaxation times prevent the development of domain-averaged temperature profiles which differ significantly from that of the reference profile (see Figure 8 and the discussion below). Perhaps such temperature profile anomalies are more conducive to the development of deep convection. In the

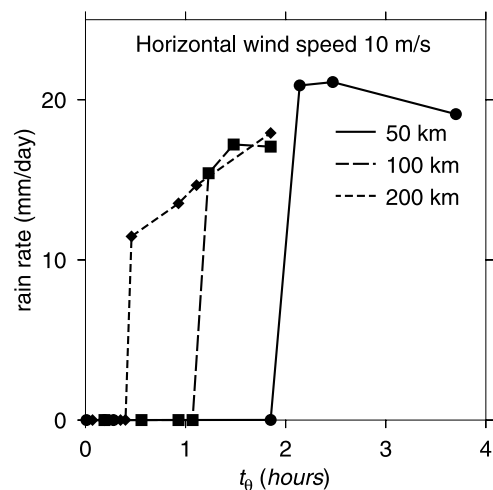


Figure 6. Equilibrium precipitation as a function of potential temperature relaxation time, t_θ , for 50, 100, and 200 km domains. The horizontal imposed wind is 10 m s^{-1} . Symbols represent numerical experiments, all of which are initially dry.

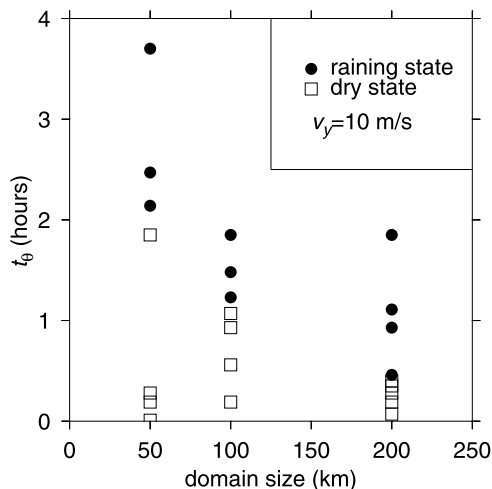


Figure 7. Simulations (shown by symbols) initiated with a dry moisture profile and with fixed surface wind speeds (v_s) of 10 m s^{-1} . Solid circles represent experiments that eventually precipitated, and open squares represent experiments which remained dry.

larger horizontal domains, these anomalies may contribute to more developed circulations which ultimately destroy the dry equilibrium state. Presumably in the presence of radiative cooling, if there is no convection and t_θ is finite, the troposphere cools which increases CAPE and decreases convective inhibition, resulting in a more favorable environment for convection.

[36] Figure 7 encapsulates the dependence of multiple equilibria on domain size and potential temperature relaxation time for given surface flux conditions. All symbols represent experiments which were initiated with completely dry profiles. Solid circles represent simulations which eventually precipitated while open squares indicate that the domain remained dry. This shows that precipitation is more likely to develop with longer relaxation times or larger domains. Furthermore, this type of plot shows the range of parameters under which our model supports multiple equilibria since we can conclude that the dry equilibrium is destroyed under the conditions which developed precipitation.

[37] We now discuss the interpretation of t_θ as a measure of the WTG approximation, and the relationship between t_θ and precipitation rate. An inspection of the vertical profile of potential temperature in the steady state suggests a nearly constant deviation from the reference profile in the free troposphere (not shown). Taking the free troposphere to be between 4 km and 12 km, we define $\delta\theta$ to be the vertical average over this height range, the horizontal average over the model domain, and the time average over the last month of the simulation. Figure 8 shows a plot of $\delta\theta$ as a function of t_θ for simulations with all ranges of surface wind speeds, all domain sizes, and arbitrary initial moisture. The black filled triangles represent the simulations which converged to the dry equilibrium, independent of model parameters, while all other symbols represent simulations which eventually sustained precipitation and are coded to indicate wind speed. There are several observations we can make from Figure 8. First note that strong convection (i.e., when convective heating is greater than radiative cooling) corresponds to $\delta\theta > 0$, with

stronger heating resulting in larger temperature deviations (indicated by steeper slopes in Figure 8). Weak or nonexistent convection results in $\delta\theta < 0$. The WTG formulation of the temperature basically guarantees this behavior; Since we parameterize the large-scale vertical advection as a relaxation (measured by t_θ), it responds to the tendencies given by radiation and convection, which implies that those control the sign of $\delta\theta$. So here we see how convection controls the temperature anomalies. However, the temperature anomalies are also known to influence convection [see, e.g., *Raymond and Sessions, 2007*], which implies a coupling between the two.

[38] To see how the coupling between convection and temperature anomalies influence precipitation rate as we vary t_θ , we plot precipitation rate versus $\delta\theta$ for all experiments (shown in Figure 9). Again we see that negative temperature deviations correspond either to the dry equilibrium (precipitation rate is zero) or to cases where convection is weak (as when the surface wind speed is equal to the ambient RCE value, in this case 5 m s^{-1}). Stronger convection associated with positive $\delta\theta$ have nonzero precipitation rates. Note that for a given surface wind speed, there is an increase in precipitation rate as the WTG approximation is relaxed (t_θ and $\delta\theta$ increase proportionally from zero), followed by a subsequent decrease. The rise corresponds to a switch from the dry equilibrium to the precipitating one, while the fall corresponds to the slower shift from a WTG-dominated simulation to one approaching RCE (as $t_\theta \rightarrow \infty$). This behavior emphasizes the coupling between the atmospheric stability and precipitation.

3.3. Dependence on Initial Conditions

[39] So far we have confirmed the existence of multiple equilibria in our CRM using the WTG approximation, and

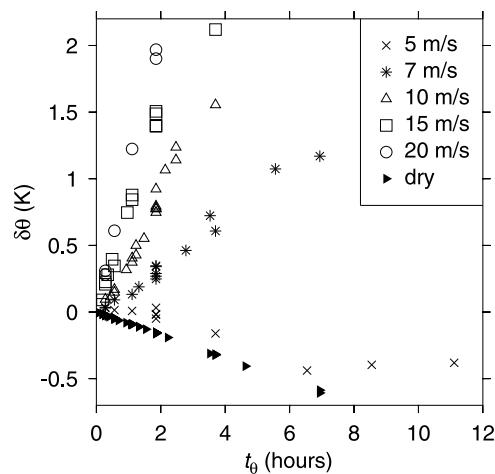


Figure 8. The $\delta\theta$ is the time and domain averaged deviation of potential temperature from RCE averaged over 4–12 km in height. In this range, $\delta\theta$ is nearly constant. Black filled triangles represent experiments which resulted in the dry equilibrium, independent of model parameters, while all other symbols correspond to experiments which evolved to the precipitating equilibrium, independent of initial moisture. For the precipitating states, the different symbols indicate the magnitude of the surface winds. For a given wind speed, the relationship between $\delta\theta$ and t_θ is nearly linear. There is also a linear relation for the nonprecipitating states.

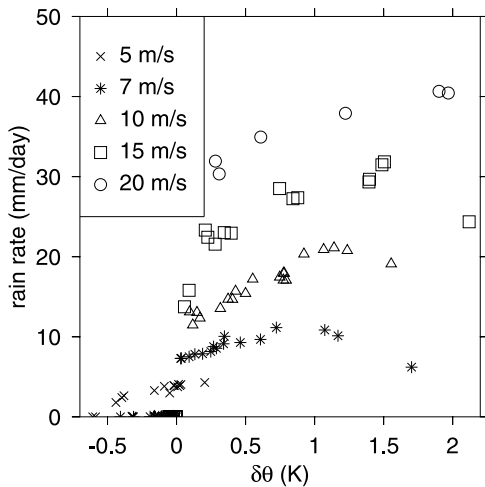


Figure 9. Precipitation rate as a function of $\delta\theta$, with the same key as in Figure 8. Nonprecipitating equilibrium states are obvious and thus have not been separately identified.

determined the range of parameters which may sustain both states. Given a specific set of boundary conditions that may sustain both equilibria, we find that the state which is ultimately realized by the model depends on the initial moisture profile of the modeled domain. This is identical to the conclusions of SBB07. SBB07 suggested that the persistence of the dry equilibrium in the presence of positive CAPE requires that the free troposphere be able to remain completely dry, even over a moist boundary layer. Though not shown, all experiments which remained dry observed this condition.

[40] To further test the sensitivity of the final equilibrium state to the initial moisture, we performed a series of experiments which were initiated with a mixing ratio profile equal to a nonzero fraction of the reference profile. We find that there is a minimum amount of moisture necessary to move the system from the nonprecipitating to the precipitating equilibrium state. An example of this is shown in Figure 10. Here, each bullet represents a simulation performed on a 50 km domain with $t_\theta = 17$ min. Line styles and symbols indicate different wind speeds. The initial moisture is taken to be a fraction of the RCE mixing ratio profile (with the fraction given by f in equation (9)). These results show that even though some simulations are initiated with nonzero moisture in the troposphere, the amount is insufficient to initiate deep convection and transition to the precipitating equilibrium. The larger the surface fluxes, the more likely a small amount of moisture will result in persistent deep convection. However, domains with low surface winds may tolerate a relatively large fraction of moisture without initiating deep convection. For example, one experiment with a wind speed of 7 m s^{-1} remained dry even with an initial moisture profile equal to 80% of the moisture of the surrounding environment. In this particular case, the initial moisture in the free troposphere rapidly vanishes due to subsidence and lateral export, which can be deduced from Figures 11 and 12.

[41] Figure 11 shows the evolution of relative humidity for the 7 m s^{-1} experiment on a 50 km domain initialized with 80% of the reference moisture profile (white is zero relative humidity, while black indicates 100%; in this experiment, $t_\theta =$

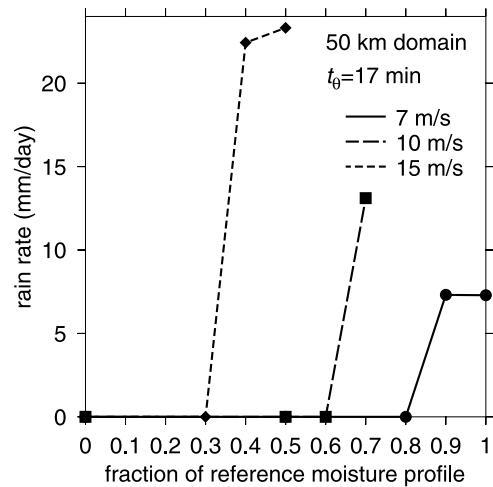


Figure 10. Simulations (shown by symbols) on a 50 km domain with $t_\theta = 17$ min. Symbols and line styles represent the sustained surface wind speeds, and the location of the bullets indicates the fraction of the RCE mixing ratio profile which was used to initiate the simulation (i.e., f in equation (9)). Here we see that in some cases the dry state is maintained even with considerable initial moistening of the free troposphere.

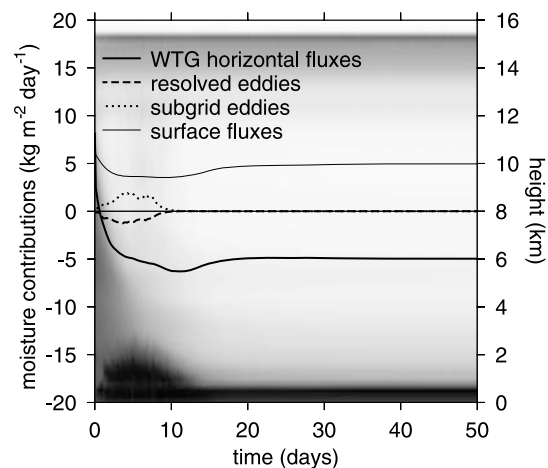


Figure 11. Image plot of the relative humidity for the 50 km domain initialized with 80% of the moisture of the surrounding environment (7 m s^{-1} surface wind, $t_\theta = 17$ min). White indicates zero, while black indicates unity. The initial moisture in the free troposphere is removed by subsidence and implied lateral export, resulting in a dry steady state. Curves indicate contributions to the total mixing ratio tendency in the free troposphere by the parameterized lateral flux of moisture and eddies. The contribution by eddies is taken as the flux through a surface at 2000 m. The thin curve shows the moisture tendency due to surface fluxes (which act to moisten the boundary layer). In the steady state, horizontal fluxes remove boundary layer moisture. Contributions to the mixing ratio have been low-pass filtered in time with a cutoff period of 1 day.

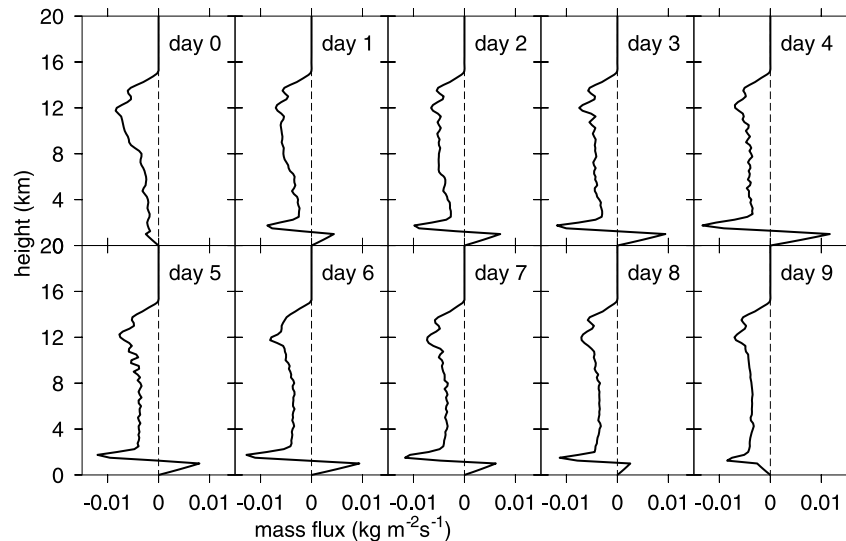


Figure 12. The vertical mass flux profile for the first 10 days of the simulation initiated with 80% of the RCE moisture profile (50 km domain, surface wind speed 7 m s^{-1} , and $t_\theta = 17 \text{ min}$). The mass flux profile changes very little in time after day 9.

17 min). Superimposed is a decomposition of the contributions of the total water mixing ratio tendencies into the free troposphere by eddy motions and parameterized lateral fluxes (the latter is due to the WTG motions given by equations (4)–(6)). We have also plotted the moisture tendency into the boundary layer from surface fluxes. Explicit and unresolved eddy contributions are taken as vertical fluxes into the free troposphere ($\overline{\rho w' r'_i}$ and $-k \partial r'_i / \partial z$, respectively; The overbar represents a horizontal average, primes indicate perturbations from the mean, w is the vertical velocity, and k is the eddy mixing coefficient given by RZ05), where we approximate the lower free tropospheric boundary to be at 2 km for this purpose. The contribution by lateral fluxes implied by WTG is vertically integrated over the entire depth, and convergence into the boundary layer is assumed to quickly enter the free troposphere. This assumption is justified by the boundary layer quasi-equilibrium hypothesis [Emanuel, 1995; Raymond, 1995]. In the first 5 days of the experiment, unresolved eddies transport moisture into the free troposphere while the resolved ones have a small drying tendency. Moisture is also removed by the WTG horizontal flux divergence. In the steady state, the horizontal fluxes remove moisture from the boundary layer (note the balance between horizontal and surface fluxes). The evolution of relative humidity in Figure 11 shows that nearly all of the initial moisture in the free troposphere is gone by day 15.

[42] Figure 12 shows the corresponding profile of vertical mass flux due to the WTG vertical velocity for the first 10 days. Each profile represents an average of the entire day. Initially, there is subsidence throughout the entire troposphere, with a maximum downdraft at 12 km. Subsequent days acquire a small updraft in the boundary layer which lies just below a sharp downdraft at about 2 km. The downdraft is a result of the strong radiative emission associated with the large moisture gradient that occurs when a dry troposphere overlies a moist boundary layer. The updraft is associated with shallow convective heating. Together, this behavior suggests a thin horizontal outflow at the level of zero mass flux

(just above 1 km). Physically, this corresponds to shallow nonprecipitating clouds mixing boundary layer air with air aloft and detraining air near cloud base, similar to the process described by Raymond and Blyth [1986]. In the model it is effected both by the subgrid mixing process and by explicit convection (see relative contributions of eddy motions to the free troposphere mixing ratio in Figure 11). The mixing process in combination with horizontal flux through the lateral boundaries removes the moisture from the free troposphere. By day 9, the system is completely subsiding. Once the moisture in the free troposphere has been evacuated, the boundary layer also becomes unsaturated, though it remains moist in the steady state. The mass flux profile changes very little from the last day plotted in Figure 12. From this we conclude that the moisture convergence in the boundary layer in the early days of the simulation is too weak to overcome convective inhibition and the troposphere dries and remains dry.

[43] The ability of our model to sustain multiple equilibria depends on the ability of shallow convection to moisten the free troposphere. The relative contributions of moisture to the free troposphere shown in Figures 11 and 14 suggest that this moistening is primarily the result of subgrid eddies. Therefore, the choice of subgrid parameterization may affect the range of parameters which permit multiple equilibria. We also note that restricting the motions to two dimensions may affect entrainment and detrainment which could further modify the parameter space permitting multiple equilibria [Petch *et al.*, 2008].

[44] Within the parameter space explored in this study, we conclude that the initial moisture determines which equilibrium state is realized, while the boundary conditions (surface wind speeds, SST, domain size and relaxation time scale in WTG mode) determine whether there are multiple equilibria.

4. NGMS as a Diagnostic

[45] Raymond *et al.* [2009] discussed the role of NGMS in transient flows as well as in a multiple equilibrium situation.

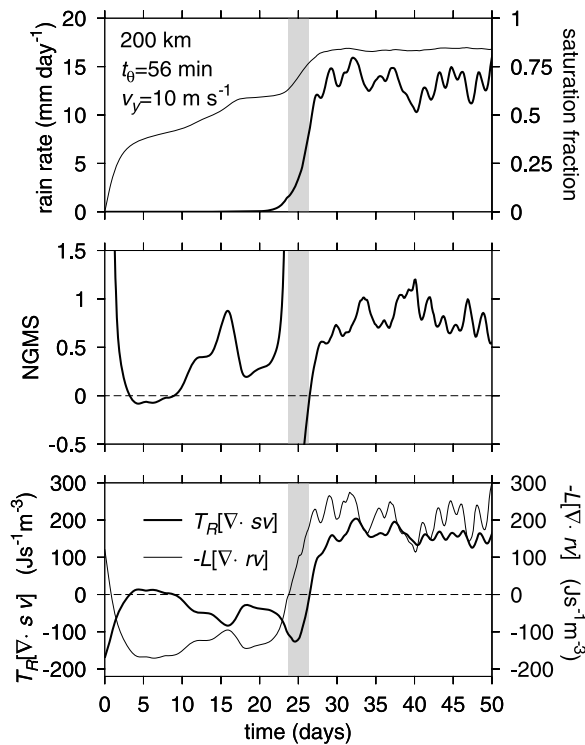


Figure 13. (top) Precipitation rate (thick curve) and saturation fraction (thin curve) as a function of time. (middle) NGMS. (bottom) Moist entropy divergence (thick curve) and moisture convergence (thin curve). Initiated with a dry atmosphere. The transition period with negative NGMS (days 24–26) is emphasized with grey shading. See text for discussion. Data shown have been low-pass filtered in time with a cutoff period of 1 day.

In this section, we study the evolution of the NGMS in the various model integrations in order to gain further insight into the nature of the equilibria and the transitions between them. Of particular interest is the possibility of a negative NGMS, which may occur during periods of rapid change in the environmental state or in a dry equilibrium steady state.

4.1. NGMS in Transient Flows

[46] The nature of the experiments reported here provides an opportunity to consider situations which make a transition from a dry to precipitating state or vice versa. The former case is encountered in an initially dry atmosphere in which the troposphere proceeds to moisten and the system initiates and sustains deep convection. During such an evolution, the initial convective vertical mass flux profile typically has a maximum at lower levels. By mass continuity, this suggests that the mass convergence is concentrated near the surface, where the moist entropy is greater than at middle levels [Raymond *et al.*, 2009]. Alternatively, the radiative cooling profile can cause a net inflow at high levels where moist entropy is large compared to midlevels (this happens in our simulations; see e.g., Figure 15). A vertical pressure integral under either of these conditions results in a net import of moist entropy. Furthermore, moisture is likely to be imported under such conditions, which implies a period where the system has negative NGMS [Sobel, 2007]. An example of the

transition from a dry state to a precipitating one is shown in Figures 13 and 14. Here, the saturation fraction increases gradually (Figure 13) as moisture begins to penetrate into the lower free troposphere (Figure 14). As seen in Figure 14, unresolved eddies associated with shallow convection are largely responsible for the initial moistening. During this period, the resolved eddies which represent the mesoscale response to the convection, actually act to dry the free troposphere. The net result, however, is moisture penetrating into the free troposphere which is accompanied by an increase in the saturation fraction. After about 24 days of the simulation, a sharp increase in the saturation fraction triggers the onset of precipitation. At this time, a change in the implicit large-scale divergence profile associated with the convective heating causes the descent in the lower free troposphere to weaken, which in turn causes the net moisture convergence ($-\nabla \cdot \mathbf{r}\mathbf{v}$) to go from negative to positive. Consequently, the NGMS (see equation (7)) goes from large and positive to large and negative. For a period of about 2.5 days, the domain is importing both moisture and moist entropy. When the system begins to export moist entropy ($[\nabla \cdot \mathbf{s}\mathbf{v}]$ goes from negative to positive), the saturation fraction and precipitation rate level off. In this case, the steady state is exporting moist entropy, importing moisture, resulting in a positive NGMS in the precipitating equilibrium.

[47] Figure 15 shows the evolution of the vertical mass flux (left) and moist entropy (right) for days 22–27 of the simulation, during which the domain makes the transition from the dry to the precipitating state. This progression begins with a descent throughout the troposphere with a maximum near 2 km and small updraft near the surface, indicating detrainment just above 1 km in height. At this time, moisture is being exported from the domain, and there is a net import of moist entropy due to the circulation near the surface. During the

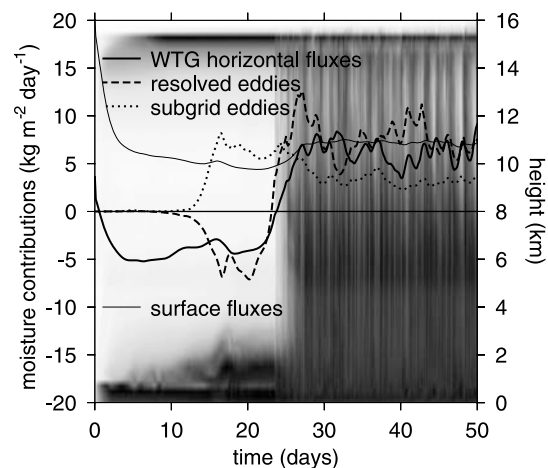


Figure 14. Domain averages of relative humidity (white indicates zero, while black is 100%) and the contribution of mixing ratio to the free troposphere by eddies and the parameterized lateral flux of moisture. The eddy contributions are taken to be fluxes through a surface above the boundary layer (2000 m). The thin curve is the mixing ratio tendency into the boundary layer by surface fluxes. The large initial tendency due to surface fluxes shows a rapid moistening of an initially dry boundary layer. Contributions to mixing ratio have been low-pass filtered in time with a cutoff period of 1 day.

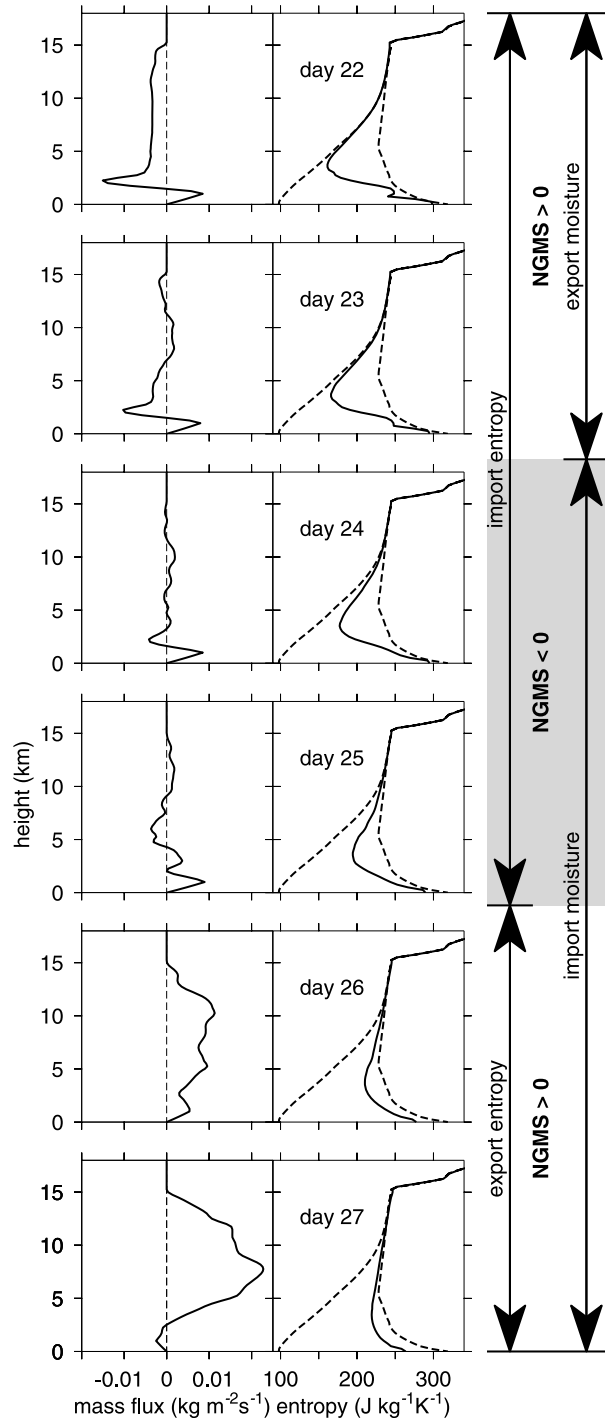


Figure 15. (left) Vertical mass flux profiles and (middle) moist entropy for days 22–27 of the simulation shown in Figure 13. Dashed curves in the entropy plot are the dry (left curve) and saturated (right curve) entropy profiles averaged over days 22–27. Days 24–25 represent time periods where the NGMS is negative. Note the rapid transition in moist entropy during this time. (right) Arrow diagrams show the time periods where entropy and moisture are imported or exported. The grey shading corresponds to the period of negative NGMS.

period with negative NGMS (days 24–25), there is very little average vertical motion in the free troposphere (which indicates the existence of some convective updrafts, whose condensation heating balances radiative cooling), and the low-level downdraft decays which weakens the divergence near the surface, allowing moisture from the boundary layer to penetrate into the free troposphere. On day 25, levels of convergence (surface, 9 km altitude) import higher values of moist entropy than exported at the levels of divergence (4 km), thus maintaining the import of moist entropy. By day 26, there is upward vertical motion from the surface to the tropopause, which progresses to strong convergence near 2.5 km. The final stages produce a net export of moist entropy (and $NGMS > 0$).

[48] In addition to convection developing in a quiescent region, negative NGMS can also occur in decaying convection as might be expected with entrainment of dry air as in work by *Sobel and Bellon* [2008]. In our simulations, this could happen for instance if a system is initiated with a moisture profile representative of the surrounding environment, but with surface wind speeds less than the value used for calculating RCE, or if the initiated moisture is insufficient to sustain convection (as in the case shown in Figures 11 and 12). Figure 16 is an example of the first possibility. In this case, we see moisture is imported into the tropospheric column; rainfall rate drops along with the saturation fraction, and NGMS is negative until the domain begins to export

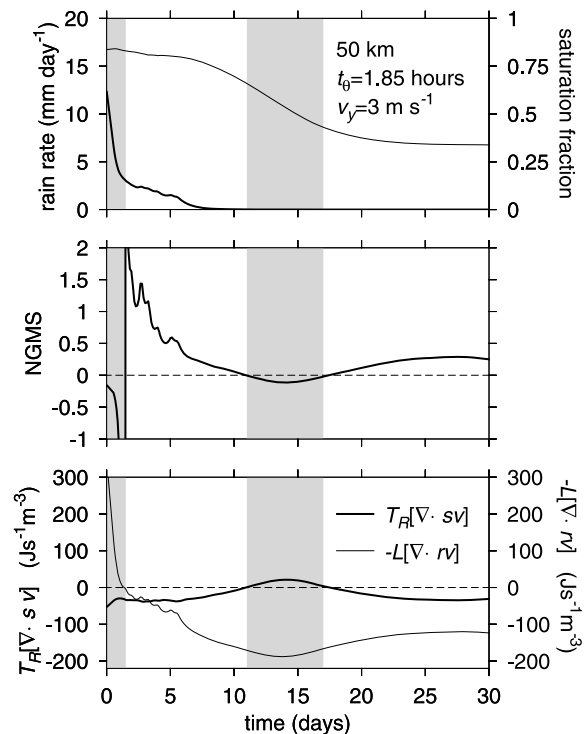


Figure 16. (top) Precipitation rate (thick curve) and saturation fraction (thin curve) as a function of time. (middle) NGMS. (bottom) Moist entropy divergence (thick curve) and moisture convergence (thin curve). Initiated with moisture profile of surrounding atmosphere. See text for discussion. Data shown have been low-pass filtered with a cutoff period of 1 day.

moisture. We note that the precipitation rate is calculated as a time derivative of the cumulative precipitation in the domain. The initial precipitation rate is artificially high since it is near an end point in the centered difference scheme used in the derivative calculation. This does not affect the calculation of NGMS. At day 11, moist entropy is exported for a period of about 3 days, again resulting in a negative NGMS. Note that the period of negative NGMS is associated with a strong time derivative of the saturation fraction. The decrease in saturation fraction is a result of the export of moist entropy. In the steady state, surface fluxes and radiation balance the import/export of moist entropy which results in a steady saturation fraction and a small NGMS (which is positive in this case). The evolution of mass flux and domain averaged moist entropy for the first 16 days of this simulation is shown in Figure 17. Times where moisture and moist entropy are imported/exported are emphasized along with the corresponding sign of NGMS. An interesting observation from this time sequence is that the atmosphere near the surface is close to saturation for times when the lateral export of moist entropy is increasing; as this quantity decreases, the atmosphere just above the surface becomes unsaturated. This implies that the surface fluxes are responsible for the negative NGMS during days 11–17.

[49] So we see in both developing and decaying stages of deep convection, NGMS may become negative. It seems that NGMS tends to become negative during times of rapid change in the modeled atmospheric state.

[50] The sign of NGMS in the transient stages of convection is particularly salient with respect to observations reported by *López-Carrillo and Raymond* [2005] and *Back and Bretherton* [2006]. *Back and Bretherton* [2006] considered the moist static energy budget (an alternative to moist entropy), and found that the sign of moist static energy export was determined by the strength of the contribution due to horizontal motions in comparison to the vertical contribution. While horizontal motions import moist static energy to the west and east Pacific, vertical motions imported moist static energy in the west Pacific and exported it from the east Pacific. The sign of the total import in the east Pacific changed depending on the size of the import by horizontal motions. Both *Back and Bretherton* [2006] and *López-Carrillo and Raymond* [2005] conclude that import or export of thermodynamic quantities by vertical motions (which contribute to the sign of NGMS) are determined by the shape of the vertical motion profile. Our results support these conclusions.

4.2. NGMS in Steady State

[51] Now we consider the steady state NGMS as a diagnostic for characterizing the equilibrium state. For example, Figure 3 compares the steady state values of NGMS for the two equilibrium states for the 50 km domains (500 m and 1 km grid resolutions). In the case where a single equilibrium exists (either dry or precipitating), the steady state NGMS is the same for both sets of experiments, independent of the initial moisture profile. In the range of wind speeds where both equilibria exist, the value of NGMS for the precipitating state is considerably larger than that of the dry state, and we can see that NGMS provides a valuable characterization of the environmental flows. Note that the value of NGMS for a surface wind speed of 5 m s^{-1} is either very large or very small

for the precipitating equilibrium, depending on grid resolution (Figure 3). We know that RCE is a possible solution for these boundary conditions, so we might expect the WTG model to reach that solution. In that case, NGMS would be undefined since there is already a balance in moisture and moist entropy, and a time average of the entrainment or detrainment of these quantities should be close to zero and their ratio undefined. However, that need not occur exactly, so instead we see large fluctuations in NGMS at this wind speed. For this reason, we exclude calculations of NGMS in WTG simulations with surface winds of 5 m s^{-1} (or, more generally, under RCE boundary conditions). For wind speeds greater than or less than 5 m s^{-1} , either convective updrafts or subsidence dominates, which implies nonzero averages of moisture and moist entropy convergence. Thus, for non-RCE boundary conditions, NGMS computed from time-averaged quantities is useful (and we emphasize that the time average is performed before the ratio of entropy divergence to moisture convergence is taken). There was one exception to this in our simulations. The 50 km domain with 1 km grid resolution sustained convection with wind speeds less than 5 m s^{-1} . We are not sure why this happens, but it also causes large fluctuations in NGMS due to the fluctuations between moisture import and export. Consequently, we also exclude these values of NGMS.

[52] To further demonstrate the value of NGMS as a diagnostic, Figure 18 shows a scatterplot of precipitation rate as a function of NGMS for all experiments with surface winds greater than 5 m s^{-1} . Those with surface winds of 5 m s^{-1} are excluded since there is essentially no correlation between the NGMS and precipitation for the reason discussed above. The experiments with wind speeds less than 5 m s^{-1} are dry in the steady state, with NGMS values less than 0.25. The symbols indicate the prescribed surface wind speed in the particular experiment. Each symbol represents the steady state rain rate and NGMS, independent of the initial moisture and domain size. There are three striking observations from Figure 18. First, all simulations which resulted in a dry equilibrium have an NGMS less than 0.25, while those in the convecting equilibrium state have an NGMS greater than 0.35. A vertical line corresponding to $\Gamma = 0.3$ clearly divides the precipitating and dry equilibria.

[53] The sharp transition in NGMS for the precipitating versus nonprecipitating equilibrium states could be related to the *Peters and Neelin* [2006] [see also *Neelin et al.*, 2009] hypothesis that the tropical atmosphere represents an observable example of self-organized criticality. Though further work is necessary to verify this in the context of our CRM, the current work suggests that NGMS could be an important parameter for understanding this phenomenon. Furthermore, the WTG approximation could prove to be important for probing this possibility numerically.

[54] *Raymond and Sessions* [2007] showed that increasing the atmospheric stability or moisture of the reference profile decreases NGMS and increases the precipitation rate for a given set of boundary conditions. Results from that work showed that the highest precipitation rates corresponded to values of NGMS which would be characterized by the dry equilibrium in this work (i.e., $\text{NGMS} < 0.2$). This suggests that the reference profiles also influence the range of boundary conditions which support multiple equilibria. More specifically, this implies that the value of NGMS which

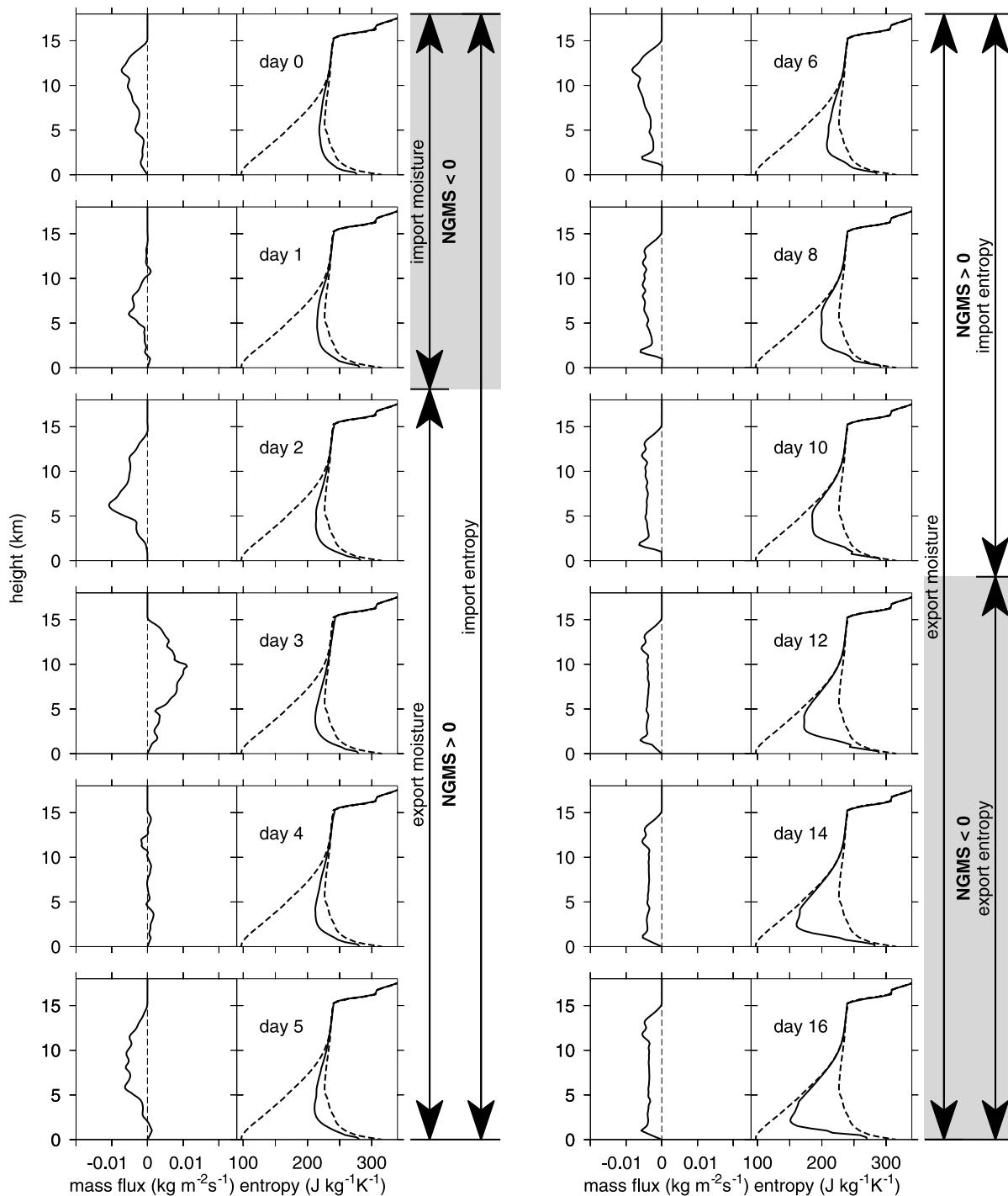


Figure 17. For each day, on the left are vertical mass flux profiles and on the right are moist entropy for days 0–6, 8, 10, 12, 14, and 16 of the simulation shown in Figure 16. Dashed curves in the entropy plot are the dry (left curve) and saturated (right curve) entropy profiles averaged over days 0–16. Grey shaded regions emphasize the time periods where the NGMS is negative. Arrow diagrams indicate periods of import or export of moisture and moist entropy.

separates the two equilibria depends on the surrounding environment. Therefore, the dashed curve in Figure 18 is valid only for a RCE reference profile. We expect that the location of this curve will change for different reference profiles.

[55] The second observation to make from Figure 18 is that, for simulations which sustain convection and precipitation, the precipitation rate increases as NGMS decreases for a given wind speed. The multiple values of rain rate for a given wind speed are a result of the different values of the potential

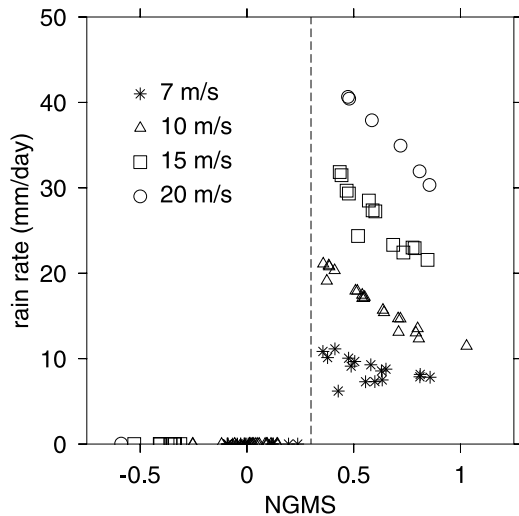


Figure 18. Steady state rain rate and NGMS (both denoted by symbols) for numerical experiments with prescribed surface winds greater than 5 m s^{-1} . The different symbols represent the strength of the surface winds. A vertical line at $\Gamma = 0.3$ clearly separates the experiments with a dry equilibrium (zero precipitation) from the precipitating equilibrium (precipitation greater than zero).

temperature relaxation time scale, t_θ (see discussion in section 3). Furthermore, the precipitation for a given value of NGMS increases with wind speed. The qualitative relationship between precipitation, NGMS and surface fluxes as shown in Figure 18 agrees with the steady state condition given by equation (8). Also note that while there is a relationship between NGMS and precipitation within an individual set of simulations, across all sets there is none, except for the split between the two types of equilibrium.

[56] The final observation regarding data in Figure 18 is that for simulations which resulted in a dry equilibrium, NGMS can be either weakly positive or negative. In all cases, subsidence results in moisture export, and therefore the sign of NGMS in the dry equilibrium is determined by whether the moist entropy is imported or exported. Near-surface circulations determine this. Negative values of NGMS have been previously reported in RCE simulations by *Bretherton et al.* [2005]. In that work, randomly seeded convection self-organized into a single intensely convecting region surrounded by a dry subsiding atmosphere. The most intensely convecting regions exhibited a positive gross moist stability, while negative values existed elsewhere. Comparing those results to the steady state NGMS values in our simulations suggests that there is indeed an analogy between the dry and convecting regions in *Bretherton et al.*'s [2005] large RCE domain and our domain-wide dry or moist WTG equilibria (this was also pointed out by SBB07).

[57] *Raymond et al.* [2009] also addressed the role of NGMS in the steady state for multiple equilibria. The authors discussed the idea of having two stable equilibria, one dry and one with persistent deep convection and precipitation, separated by an unstable equilibrium. Figure 19 is the conceptual picture from *Raymond et al.* [2009], reprinted here for convenience. The existence and location of the unstable equilibrium relative to the stable equilibrium is

dependent on the boundary conditions. Initial conditions and the amplitude of external forcing, if any, determine the state of the system relative to the unstable equilibrium, and hence which equilibrium is ultimately realized in the steady state.

5. Summary and Discussion

[58] We have established the existence of a dry and a precipitating steady state in a cloud-resolving model employing the WTG approximation. In this study, we have identified several parameters which control the existence of two equilibrium states: (1) surface fluxes (modulated by SST or surface winds), (2) domain size, and (3) time scale for relaxation of the potential temperature to the environmental mean. Our results suggest that certain combinations of these are necessary for supporting multiple equilibria, and provide some guidance for atmospheric conditions that may also be good candidates for multiple equilibrium states.

[59] Given an initially dry environment, the ability of the domain to initiate and sustain deep convection hinges on its capacity to moisten the free troposphere in the face of radiatively induced subsidence and maintain a sufficient saturation fraction. As shown in numerous studies [*Bretherton et al.*, 2004; *Raymond et al.*, 2007], the precipitation is a sensitive function of moisture in the environment, so in order for deep convection to develop, there must be an external source of moisture and a mechanism which serves to transport that moisture into the troposphere. Moisture from the boundary layer is accessible as long as convection can overcome convective inhibition. The most effective channel for this is increasing surface fluxes. Alternatively, some conditions may be conducive to the initiation and development of deep convection, such as regions of low convective inhibition (as occurs with larger domain sizes). Thus, increasing the domain size will increase the likelihood that convection will occur spontaneously and allow the troposphere to tap into the moisture of the boundary layer. In addition to boundary layer moisture, atmospheric circulations can horizontally advect moisture from the surrounding environment, providing an alternate mechanism for the system to transition from the dry state to the precipitating one. This mechanism is likely influenced by the potential temperature relaxation time, t_θ ,

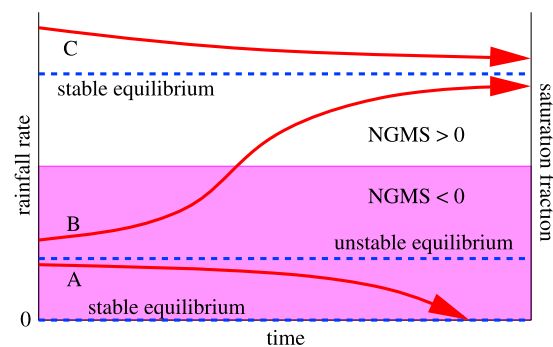


Figure 19. Two stable equilibria, one representing a precipitating state with $\text{NGMS} > 0$ and one with zero precipitation and $\text{NGMS} < 0$. An unstable equilibrium separates these two, and the state ultimately realized by the system will depend on the initial conditions. Previously published as Figure 8 of *Raymond et al.* [2009].

since this controls the parameterized large-scale vertical motion. By mass continuity, this also affects horizontal flows which may advect moisture. Our results indicate that larger values of t_θ permit the free tropospheric moistening necessary to initiate deep convection. These results are qualitatively consistent with the dependence of multiple equilibria on the moisture relaxation time used by SBB07. In the work by SBB07, longer relaxation times for moisture advection killed the dry equilibrium state. If any of these mechanisms successfully bring the system to the convecting equilibrium from a completely dry state, we assume the conditions are insufficient to sustain a dry equilibrium. Failure, on the other hand, implies the existence of multiple equilibria under the specific set of boundary conditions.

[60] It is important to also point out that the dependence on the time scale for relaxation of the local potential temperature profiles to the large-scale mean suggests that nonlocal adjustment, parameterized here by the weak temperature gradient approximation, is an important ingredient in producing multiple equilibria. Our results clearly show that if the WTG approximation is only weakly obeyed (as measured by the magnitude of t_θ), the dry equilibrium is destroyed. The multiple equilibria are local phenomena which occur over areas small compared to some nominal larger domain (outside the computational domain, and thus implicit in our calculations), with the mass circulation implied by the WTG vertical velocity closed everywhere in the domain. A dry equilibrium cannot occur in the spatial average over a domain with a truly closed mass budget (represented by RCE) since in that case deep convection must occur in order to provide heating to balance radiative cooling.

[61] Upon establishing a set of boundary conditions capable of supporting multiple equilibria, the actual state realized by the model will depend on the initial moisture in the free troposphere. In this case, there is a threshold fraction of the mixing ratio profile below which the initial moisture is advected out and the system sits at the dry equilibrium. Moisture profiles which exceed the threshold fraction can sustain a convecting equilibrium. The threshold value is a function of boundary conditions, being small for conditions which support heavy precipitation (as with large surface winds) and large in conditions which result in smaller precipitation rates.

[62] Finally, we consider NGMS as a diagnostic of environmental characteristics. In the steady state, this set of simulations found that values of NGMS less than 0.25 correspond to the dry equilibrium, while values greater than 0.35 all correspond to a precipitating equilibrium. The dry equilibrium physically represents a region of subsidence where moisture is being exported from the domain and there is relatively little exchange of moist entropy between the modeled domain and the surrounding environment, giving rise to the smaller magnitudes of NGMS. Under these conditions, the vertical integral of moist entropy can give a net import or export, depending on circulations in the boundary layer. Completely divergent mass flux profiles imply net entropy export which, when coupled to moisture export, implies a negative value of NGMS in the steady state. Any convergence in the boundary layer is sufficient to import moist entropy and result in a small, positive NGMS.

[63] The NGMS also provides insight with respect to transient stages of developing or decaying deep convection. When convection is developing in an initially dry environ-

ment, the domain goes from having a net export of moisture to a net import. Furthermore, the moist entropy convergence of the dry state transitions to a net divergence in the mature stages of convection. As these sign changes need not occur simultaneously, there may be a period of time when both moisture and moist entropy are being imported, resulting in a negative value of NGMS. A similar argument holds also for decaying convection, in which case the period of negative NGMS corresponds to both quantities being exported. Our simulations showed that periods of negative NGMS correspond to times of rapid change in the saturation fraction.

Appendix A: Initialization of Thermodynamic Profiles

[64] As mentioned in section 2, the initial potential temperature profile is given by

$$\theta_{\text{init}} = \theta_0(1 + \delta\theta_{\text{local}}/\theta_0)(1 + \delta\theta_{\text{random}}/\theta_0), \quad (\text{A1})$$

where θ_0 is the height-dependent RCE profile used to represent the large-scale mean, $\delta\theta_{\text{local}}$ and $\delta\theta_{\text{random}}$ represent localized and random perturbations, respectively,

$$\delta\theta_{\text{local}} = \delta\theta_{\text{local}}^{\text{max}} \exp[-(x_s^2 + z_s^2)] \quad (\text{A2})$$

$$\delta\theta_{\text{random}} = \delta\theta_{\text{random}}^{\text{max}} z_s \exp[1 - z_s]$$

Here, x_s and z_s are scaled Cartesian coordinates (i.e., $z_s = z/z_{\text{scale}}$, where z_{scale} defines the width of the localized Gaussian perturbation; an analogous definition holds for x_s). For most simulations, $x_{\text{scale}} = 3$ km, $z_{\text{scale}} = 1$ km. The maximum values of the perturbations are given by $\delta\theta_{\text{local}}^{\text{max}} = f_{\text{local}}\theta_0$ and $\delta\theta_{\text{random}}^{\text{max}} = f_{\text{random}}\theta_0$, where f_{local} and f_{random} are fractional multipliers which represent the actual model input. The maximum magnitude of $\delta\theta_{\text{local}}^{\text{max}}$ and $\delta\theta_{\text{random}}^{\text{max}}$ are approximated below by multiplying the respective fractional multipliers by 300 K. We prescribe random temperature fluctuations with a maximum magnitude of $\delta\theta_{\text{random}}^{\text{max}} = 0.3$ K to be distributed at 1 km in altitude. Similarly, setting $\delta\theta_{\text{local}}^{\text{max}} = 9$ K increases the local temperature for a 3 km region centered horizontally with a vertical extent of about 1 km centered at 1 km in altitude. We originally chose such a large perturbation in hopes that we could get a reliable response (either developing precipitation or not) from an initially dry domain.

[65] A limited number of simulations which vary $\delta\theta_{\text{local}}^{\text{max}}$ and $\delta\theta_{\text{random}}^{\text{max}}$ were performed to determine the sensitivity to initial conditions. While preliminary results suggest that the final state of the system is not very sensitive to these perturbations, two sets of experiments suggest that the initial conditions play some role in the equilibration time of the model. Specifically, as noted in section 2, there were two experiments in which the free troposphere moistened but convective inhibition suppressed the development of deep convection even after running the simulation for a full year. In these cases, the precipitation rate remained negligible compared to the corresponding rate in the equilibrium state with persistent deep convection, but the NGMS remained noisy up until the last month of the simulation. Repeating these experiments with slightly different initial conditions (i.e., adjusting $\delta\theta_{\text{local}}$ and $\delta\theta_{\text{random}}$) allowed the model to equilibrate quicker, but did not change the final state of the system.

[66] More investigation is necessary to conclusively determine the sensitivity of the final state on the initial potential temperature perturbations. As stated in section 2, setting $\delta\theta_{\text{random}}^{\text{max}} = \delta\theta_{\text{local}}^{\text{max}} = 0$ and $f = 0$ (where f is defined in equation (9)) will not generate convection no matter what the boundary conditions are.

[67] **Acknowledgments.** We would like to thank two anonymous reviewers whose helpful comments improved this manuscript. This research was supported in part by the State of New Mexico through resources provided by the New Mexico Computing Applications Center. This work was also supported by U.S. National Science Foundation grants ATM-0638801 and ATM-0542736.

References

- Back, L. E., and C. S. Bretherton (2006), Geographic variability in the export of moist static energy and vertical motion profiles in the tropical Pacific, *Geophys. Res. Lett.*, *33*, L17810, doi:10.1029/2006GL026672.
- Bellon, G., and A. H. Sobel (2010), Multiple equilibria of the Hadley circulation in an intermediate-complexity axisymmetric model, *J. Clim.*, *25*, 1760–1778.
- Bretherton, C. S., and P. K. Smolarkiewicz (1989), Gravity waves, compensating subsidence and detrainment around cumulus clouds, *J. Atmos. Sci.*, *46*, 740–759.
- Bretherton, C. S., M. E. Peters, and L. E. Back (2004), Relationships between water vapor path and precipitation over the tropical oceans, *J. Clim.*, *17*, 1517–1528.
- Bretherton, C. S., P. N. Blossey, and M. Khairoutdinov (2005), An energy-balance analysis of deep convective self-aggregation above uniform SST, *J. Atmos. Sci.*, *62*, 4273–4292.
- Emanuel, K. (1995), The behavior of a simple hurricane model using a convective scheme based on subcloud-layer entropy equilibrium, *J. Atmos. Sci.*, *52*, 3960–3968.
- López-Carrillo, C., and D. J. Raymond (2005), Moisture tendency equations in a tropical atmosphere, *J. Atmos. Sci.*, *62*, 1601–1613.
- Mapes, B. E., and R. H. Houze Jr. (1995), Diabatic divergence profiles in western Pacific mesoscale convective systems, *J. Atmos. Sci.*, *52*, 1807–1828.
- Neelin, J. D., and I. M. Held (1987), Modeling tropical convergence based on the moist static energy budget, *Mon. Weather Rev.*, *115*, 3–12.
- Neelin, J. D., O. Peters, and K. Hales (2009), The transition to strong convection, *J. Atmos. Sci.*, *66*, 1665–1683, doi:10.1175/2008JAS2806.1.
- Petch, J. C., P. N. Blossey, and C. S. Bretherton (2008), Differences in the lower troposphere in two- and three-dimensional cloud-resolving model simulations of deep convection, *Q. J. R. Meteorol. Soc.*, *134*, 1941–1946.
- Peters, O., and J. D. Neelin (2006), Critical phenomena in atmospheric precipitation, *Nat. Phys.*, *2*, 393–396, doi:10.1038/nphys314.
- Raymond, D. J. (1995), Regulation of moist convection over the west Pacific warm pool, *J. Atmos. Sci.*, *52*, 3945–3959.
- Raymond, D. J., and A. M. Blyth (1986), A stochastic mixing model for nonprecipitating cumulus clouds, *J. Atmos. Sci.*, *43*, 2708–2718.
- Raymond, D. J., and S. L. Sessions (2007), Evolution of convection during tropical cyclogenesis, *Geophys. Res. Lett.*, *34*, L06811, doi:10.1029/2006GL028607.
- Raymond, D. J., and X. Zeng (2000), Instability and large scale circulations in a two-column model of the tropical troposphere, *Q. J. R. Meteorol. Soc.*, *126*, 3117–3135.
- Raymond, D. J., and X. Zeng (2005), Modelling tropical atmospheric convection in the context of the weak temperature gradient approximation, *Q. J. R. Meteorol. Soc.*, *131*, 1301–1320.
- Raymond, D. J., G. B. Raga, C. S. Bretherton, J. Molinari, C. López-Carrillo, and Ž. Fuchs (2003), Convective forcing in the intertropical convergence zone of the east Pacific, *J. Atmos. Sci.*, *60*, 2064–2082.
- Raymond, D. J., S. L. Sessions, and Ž. Fuchs (2007), A theory for the spinup of tropical depressions, *Q. J. R. Meteorol. Soc.*, *133*, 1743–1754.
- Raymond, D. J., S. L. Sessions, A. H. Sobel, and Ž. Fuchs (2009), The mechanics of gross moist stability, *J. Adv. Model Earth Syst.*, *1*(9), 20 pp., doi:10.3894/JAMES.2009.1.9.
- Sobel, A. H. (2007), Simple models of ensemble-averaged tropical precipitation and surface wind, given the sea surface temperature, in *The Global Circulation of the Atmosphere*, edited by T. Schneider and A. H. Sobel, pp. 219–251, Princeton Univ. Press, Princeton, N. J.
- Sobel, A. H., and G. Bellon (2008), The effect of imposed drying on parameterized deep convection, *J. Atmos. Sci.*, *66*, 2085–2096.
- Sobel, A. H., and C. S. Bretherton (2000), Modeling tropical precipitation in a single column, *J. Clim.*, *13*, 4378–4392.
- Sobel, A. H., G. Bellon, and J. Bacmeister (2007), Multiple equilibria in a single-column model of the tropical atmosphere, *Geophys. Res. Lett.*, *34*, L22804, doi:10.1029/2007GL031320.

D. J. Raymond, S. L. Sessions, and S. Sugaya, Department of Physics, New Mexico Institute of Mining and Technology, 801 Leroy Pl., Socorro, NM 87801, USA. (sessions@kestrel.nmt.edu)

A. H. Sobel, Department of Applied Physics and Applied Mathematics, Columbia University, S.W. Mudd, Rm. 217, 500 West 120th St., New York, NY 10027, USA.